Influence of the boundary conditions on the *H*-mode power threshold

D. Kalupin,[a] M. Z. Tokar, B. Unterberg, and X. Loozen
Institut für Plasmaphysik, Forschungszentrum Jülich GmbH, EURATOM Association, D-52425 Jülich, Germany, partner in Trilateral Euregio Cluster

D. Pilipenko
Université Libre de Bruxelles, CP 231 Boulevard Du Triomphe, Association EURATOM- Etat Belge, B-1050, Bruxelles, Belgium

R. Zagorski and TEXTOR Contributors
Institute of Plasma Physics and Laser Microfusion, EURATOM Association, 00-908 Warsaw, Poland

(Received 22 September 2005; accepted 18 January 2006; published online 16 March 2006)

The effect of boundary conditions at the last closed magnetic surface (LCMS) on the formation of the edge transport barrier (ETB) in tokamaks is investigated by one-dimensional transport calculations for the radial profiles of plasma parameters. For a given heating power the transition from the low confinement mode (*L* mode) to the high confinement mode (*H* mode) can be triggered by increasing the density *e*-folding length, δ_n, or reducing the temperature *e*-folding length, δ_T, at the LCMS. This is explained by the decrease of heat losses from the confined plasma with the convection of charged particles and changeover to the case where losses are mostly due to heat conduction. In such a case, corresponding to a divertor configuration, the computed power threshold for the *L*- to *H*-mode transition (*L-H* transition) is in a good agreement with the experimental multimachine scaling. © *2006 American Institute of Physics*. [DOI: 10.1063/1.2178176]

I. INTRODUCTION

Recently, the one-dimensional code RITM (radiation by impurities in the transport model)[1–4] has been significantly amended by including a model for the edge transport, which reproduces the formation of the edge transport barrier (ETB), and was applied for a self-consistent modeling of the *H*-mode plasmas in the tokamak JET (Joint European Torus[3,4]). The present paper is an extension of studies done in Ref. 4 aimed to specify the dependencies of the *L-H* threshold power on the boundary conditions.

The experimentally established multimachine scaling for the *H*-mode power threshold[5] predicts that the transition to the *H* mode takes place when the total power transported through the last closed magnetic surface (LCMS) exceeds the critical level in megawatts,

$$P_{\mathrm{th}} = 0.042 \bar{n}_e^{0.64} B^{0.78} S^{0.94}, \tag{1}$$

where $\bar{n}_e$ is the line averaged electron density in 10^{20} m^{-3}, *S* the plasma surface area in m^2, and *B* the toroidal magnetic field in Torr. At the same time, there are experiments where the significant deviation of the threshold power from this scaling was observed. In particular, the onset of the *H* mode at a low density or in a limiter configuration requires usually a significantly higher power than the scaling predicts.[6–8]

II. BIFURCATION TO THE IMPROVED CONFINEMENT

The transport equations solved by the code RITM and the code structure are described in detail in Refs. 1–4. Here, we analyze only qualitatively which parameters are of importance for the critical conditions. For this purpose we proceed from the global plasma heat balance by assuming that the energy is lost only by heat conduction,

$$P_{\mathrm{heat}} = P(n,T,\nabla n,\nabla T) \equiv -S\langle \chi_\perp n \nabla T \rangle. \tag{2}$$

Here, P_{heat} is the total heating power, *S* the LCMS area, $\chi_\perp = \chi_\perp^e + \chi_\perp^i$ the total plasma heat diffusivity prescribed by the transport model from Ref. 4, and electron and ion temperatures are taken the same. The angular brackets mean the averaging over the plasma edge region with the width of the neutral penetration depth,[9] $l = 1/\langle n \rangle \sigma_*$, with $\sigma_* = \sqrt{(k^{cx}+k^i)k^i}/V_{thi}$ being the cross section for neutral attenuation due to ionization in the plasma and V_{thi} the ion thermal velocity acquired by neutrals after charge exchange.

For further qualitative analysis we assumed $\langle \nabla n \rangle \approx \langle n \rangle / l$, $\langle \nabla T \rangle \approx \langle T \rangle / l$, where $\langle n \rangle \approx \bar{n}_e/2$ and the line averaged density $\bar{n}_e$ is a parameter prescribed by the discharge conditions. In this case Eq. (2) provides an equation for the averaged edge temperature or temperature gradient. As an example we consider a medium size tokamak with the minor radius 0.4 m, major radius 1.68 m, plasma current 0.3 MA, and toroidal magnetic field 1.9 T. Figure 1 displays the $P[\langle \nabla T \rangle]$ dependence for different magnitudes of the toroidal magnetic field *B* and $\bar{n}_e = 2 \times 10^{19}$ m^{-3}. In Fig. 2 this dependence is displayed for $B = 1.9$ T and different $\bar{n}_e$.

One can see that in all cases $P[\langle \nabla T \rangle]$ has an *N*-like shape that can be explained as follows. The transport model used takes into account drift instabilities of different nature, which are divided into two groups of typical "core" and "edge" modes. The first group includes contributions from toroidal ion temperature gradient (ITG) and trapped electron (TE) treated similarly to the MMM95, GLF23, and Weiland transport models.[10–12] The second one comprises instabilities

[a]Electronic mail: d.kalupin@fz-juelich.de

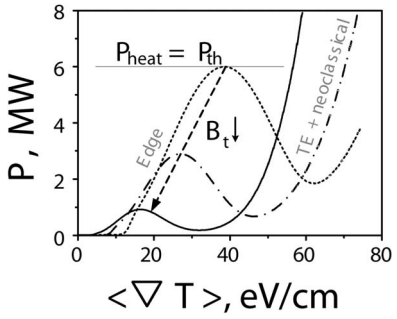

FIG. 1. Heat losses through the LCMS vs the temperature gradient at the plasma edge for different magnitudes of the magnetic field in TEXTOR: 1 T (solid curve), 2 T (chain curve), and 3 T (broken curve).

driven by collisions and current perturbations, e.g., drift-resistive ballooning and drift-Alfvén modes.[13–15] At low $\langle T\rangle$ and $\langle \nabla T\rangle$ the plasma collisionality is high; the edge mode makes a very large contribution to $\chi_\perp^i$. With increasing $\langle T\rangle$ and $\langle \nabla T\rangle$ the collisionality drops and plasma beta increases, leading to stabilization of the edge mode,[14] and P decreases. On the second part of the $P[\langle \nabla T\rangle]$ dependence, where P again monotonically grows with the temperature gradient, the transport is due to neoclassical contribution and TE mode, since the most dangerous ITG instability is suppressed by the edge density gradient.

An N-like shape of $P[\langle \nabla T\rangle]$ allows for the bifurcation between high and low transport states. Stationary $\langle T\rangle$ and $\langle \nabla T\rangle$ values are determined by the intersections of the curve $P[\langle \nabla T\rangle]$ with the horizontal line $P=P_{\text{heat}}$. At a low heating power the solution with a small temperature gradient on the brunch dominated by the edge turbulence is realized. If P_{heat} exceeds the critical level P_{th}, corresponding to the maximum of $P[\langle \nabla T\rangle]$, a bifurcation into the state with a significantly reduced transport takes place and the temperature gradient becomes sharp. This bifurcation leads to the formation of ETB and can be interpreted as the L-H transition.

A model predicting a bifurcation in the edge plasma state when the temperature gradient approaches a critical value has been previously proposed in Ref. 16, where the L-H transition was interpreted as a suppression of a macroscopic thermal instability caused by the energy losses due to neutrals and impurities. In our transport model the main transport contribution in the L mode is due to a different mechanism, namely drift-Alfvén microinstability, and the losses above are included self-consistently as sinks into transport equations. Therefore, in spite of some similarities, e.g., sharp increase in the temperature gradient when the heating power exceeds a certain threshold, our predictions differ from those of Ref. 16.

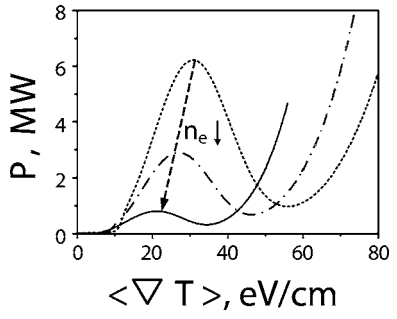

FIG. 2. Heat losses through the LCMS vs the temperature gradient at the plasma edge for different magnitudes of the plasma density 10^{13} cm^{-3} (solid curve), 1.5×10^{13} cm^{-3} (chain curve), and 2×10^{13} cm^{-3} (broken curve).

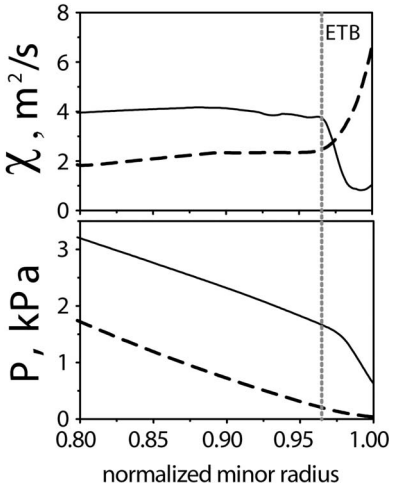

FIG. 3. Edge profiles of the ion heat transport coefficient (top) and total pressure (bottom) for L (dashed) and H mode (solid) conditions computed with the RITM code.

As can be seen from Figs. 1 and 2 by comparing the critical power for the bifurcation with that prescribed by Eq. (1), the present results agree qualitatively with the experimental findings. The model qualitatively reproduces the increase of P_{th} with the density and magnetic field predicted by the scaling. More detailed numerical comparison between model predictions and experimental values of P_{th} in the JET tokamak is given in Ref. 4.

Figure 3 shows the radial profiles of the plasma heat diffusivity and pressure calculated for a total heating power of 2.5 and 4 MW. Typical L-mode conditions are obtained at the lower power. The pressure profile at the edge is relatively flat and the turbulent transport coefficient increases towards the separatrix. With the power increased up to 4 MW a significant reduction of the transport at the edge takes place and a pronounced pedestal on the pressure profile is formatted as it takes place by the L-H transition.[17,18]

III. ROLE OF CONVECTIVE HEAT LOSSES

In the qualitative analysis in the previous section convective heat losses have been neglected. However, at the plasma edge the ionization of recycling neutrals can provide strong charged particle flow. Since neutrals are generated on divertor plates and pass through the scrape-off layer (SOL) before they enter the confined volume, a firm consideration would require a SOL description. Here, we do this parametrically by varying the e-folding lengths of the plasma density and temperature at the LCMS, δ_n and δ_T, respectively. These are taken into account in RITM calculations through the boundary conditions at $r=a$,

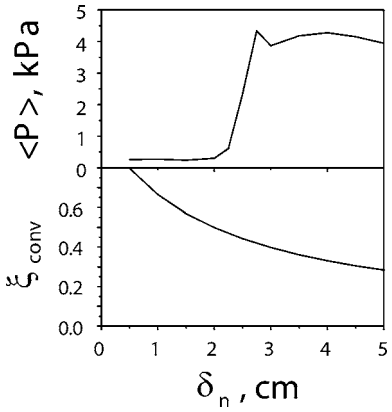

FIG. 4. Edge plasma pressure and fraction of convective heat losses at the LCMS vs the density *e*-folding length.

$$\nabla n = -n/\delta_n, \quad \nabla T = -T/\delta_T.$$

By changing δ_n and δ_T, one can simulate the switch between regimes dominated by conduction or convection heat losses. Indeed, the fraction of convective losses, $-3TD_\perp \nabla n$, in the total one, $-3TD_\perp \nabla n - \chi_\perp n \nabla T$, is given at the LCMS by the value $\xi_{\text{conv}} = (1 + \chi_\perp / 3D_\perp \delta_n / \delta_T)^{-1}$. By varying the ratio δ_n / δ_T, ξ_{conv} can be changed from 0 to 1.

Figures 4 and 5 display the averaged pressure at the pedestal top, $0.95 < \rho < 0.975$, and fraction of convective heat losses at the LCMS vs δ_n and δ_T, respectively, found for the same conditions as in Fig. 3. The ETB onset corresponds to the sudden increase of the edge pressure. For a given temperature decay length this occurs if the density decay length exceeds a certain critical value (Fig. 4). On the contrary, for a given δ_n, the reducing δ_T leads to the confinement improvement if δ_T becomes lower than a certain limit (Fig. 4). In both cases the confinement improves when the fraction of convective losses reduces below 45%. A smaller convection fraction requires a larger temperature gradient to transport a given heating power through the LCMS; when this exceeds a certain threshold the suppression of the edge turbulence and improvement of confinement takes place.

The power threshold for the ETB formation under different plasma conditions is shown in Fig. 6 as a function of

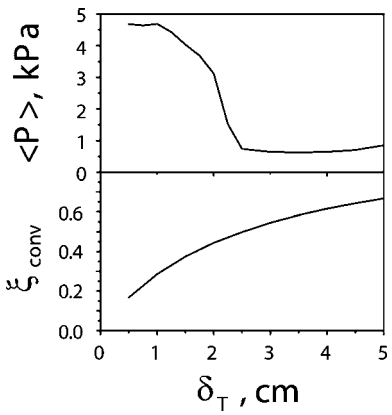

FIG. 5. Edge plasma pressure and fraction of convective heat losses at the LCMS vs the temperature *e*-folding length.

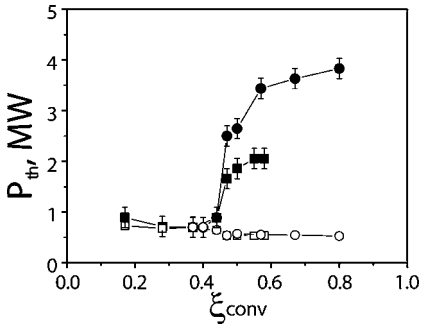

FIG. 6. *H*-mode threshold computed with RITM (black circles and boxes, corresponding to variation of δ_n and δ_T, correspondingly) and according to multimachine scaling, Eq. (1) (empty circles and boxes) vs the fraction of the convective heat losses.

ξ_{conv}. Black points show the results of RITM calculations and white ones represent the predictions of the scaling law, Eq. (1). The variation of the fraction of convective losses was done by changing the ratio δ_n / δ_T. If the fraction of convective heat losses is below 45%, the computed power coincides well with the scaling predictions. An increase of ξ_{conv} above 45% leads to a strong increase of the computed power with respect to the scaling predictions. The value of this offset depends on the particular approach to change ξ_{conv} (cycles and squares) and can be up to several megawatts.

Finally, notice that the dependence of the threshold power on the logarithmic decay lengths found above differs from that obtained in Ref. 16. First, δ_n and δ_T considered here are the values at the separatrix, which differ principally from L_n and L_T averaged over the edge layer discussed in Ref. 16. Second, according to Fig. 6 P_{th} increases step-like from the level prescribed by the intermachine scaling law when, with a fixed δ_T, δ_n decreases to a critical value. Equation (7) in Ref. 16 provides, however, a monotonic dependence of P_{th} on $L_n \sim n/\Gamma\perp$. Testing of these predictions in future experiments on tokamaks TEXTOR and JET is planned.

IV. DISCUSSION

As was already mentioned in Sec. III, the penetration of neutrals through the SOL is the process which defines the heat balance at the edge. If the SOL is transparent for neutrals, then they escape freely into the confined volume and provide a large source of charged particles there. In steady state this source should be compensated by the particle outflow driven by diffusion back into the SOL. This requires a large radial gradient of density. The convective heat flux associated with this particle outflow would dominate the heat balance at the edge, when the heat conduction cannot contribute much to the total heat flux.

In the opposite situation, when most neutrals are ionized in the SOL, the heat losses at the edge should be driven mainly by the conduction. Indeed, due to strong attenuation of the neutral flux in the SOL, only a small fraction of it would enter the confined plasma. This presumes a small charged particle outflow, and, consequently, a small amount

of heat transported through the convective channel. The conduction would be the dominant mechanism for the heat losses under these conditions.

The attenuation of the neutral flux in the SOL is determined by the ratio of the distance which neutrals should travel before they enter the confined plasma to their mean penetration length. This varies inversely proportional with the density in the SOL. Thus, the reduction of both density in the SOL and the SOL thickness, e.g., by a switch from divertor to limiter, would lead to a higher number of neutrals entering into confined plasma and increasing fraction of the convective losses.

As it appears from Fig. 6, the higher convective losses hinder the *H*-mode onset. This, particularly, can be the reason for the higher *H*-mode threshold found in limiter configurations, when the plasma column is placed very close to plasma facing components, or in low density plasmas. In both cases, the SOL is almost transparent for neutrals and strong convective heat losses set up at the edge.

V. CONCLUSIONS

For the given heating power, the transition to improved confinement occurs if the *e*-folding length of density is increased and the temperature *e*-folding length is reduced. This can be explained by the transition from the case where heat losses from the confined plasma are mostly due to charged particle convection to the situation with heat losses dominated by the conduction. In the latter situation, the computed threshold power coincides with the value predicted by the scaling law, whereas strong convective energy losses lead to the increase of the threshold power by several times compared to the multimachine scaling.

[1] M. Z. Tokar, Plasma Phys. Controlled Fusion **36**, 1819 (1994).
[2] D. Kalupin, M. Z. Tokar, P. Dumortier *et al.*, Plasma Phys. Controlled Fusion **43**, 945 (2001).
[3] B. Unterberg, D. Kalupin, M. Z. Tokar *et al.*, Plasma Phys. Controlled Fusion **46**, A241 (2004).
[4] D. Kalupin, M. Z. Tokar, B. Unterberg, X. Loozen, and D. Pilipenko, Nucl. Fusion **45**, 468 (2005).
[5] J. A. Snipes, M. Greenwald, F. Ryter *et al.*, Proceedings of the 19th IAEA Energy Conference, Lyon, 2002 (IAEA, Vienna, 2002); CD-ROM fileTERCT-P/04; http://www.iaea.org/programmes/ripc/physics/fec2002/html/fec2002.htm
[6] A. E. Hubbard, R. L. Boivun, J. F. Drake, M. Greenwald, Y. In, J. H. Irby, B. N. Rogers, and J. A. Snipes, Plasma Phys. Controlled Fusion **40**, 689 (1998).
[7] S. V. Lebedev, M. V. Andrejko, L. G. Askinazi *et al.*, Plasma Phys. Controlled Fusion **38**, 1103 (1996).
[8] C. E. Bush, S. A. Sabbagh, S. J. Zweben *et al.*, Phys. Plasmas **2**, 2366 (1995).
[9] M. Z. Tokar, Plasma Phys. Controlled Fusion **35**, 1119 (1993).
[10] G. Bateman, A. H. Kritz, J. E. Kinsey, A. J. Redd, and J. Weiland, Phys. Plasmas **5**, 1793 (1998).
[11] R. E. Waltz, G. M. Staebler, W. Dorland, G. W. Hammett, and M. Kotschenreuther, Phys. Plasmas **4**, 2482 (1997).
[12] J. Weiland, *Collective Modes in Inhomogeneous Plasma* (Institute of Physics Publishing, Bristol, 2000).
[13] P. N. Gusdar, Phys. Fluids B **B5**, 3712 (1993).
[14] W. Kerner, Yu. Igitkhanov, G. Janeschitz, and O. Pogutse, Contrib. Plasma Phys. **38**, 118 (1998).
[15] G. Janeschitz, G. W. Pacher, Yu. Igitkhanov, H. D. Pacher, S. D. Pinches, O. Pogutse, and M. Sugihara, J. Nucl. Mater. **266–269**, 843 (1999).
[16] W. M. Stacey, Phys. Plasmas **9**, 3082 (2002).
[17] R. J. Groebner, M. A. Mahdavi, A. W. Leonard, T. H. Osborne, and G. D. Porter, Plasma Phys. Controlled Fusion **44**, A265 (2002).
[18] T. Hatae, M. Sugihara, A. E. Hubbard *et al.*, Nucl. Fusion **41**, 285 (2001).